Hole-initiated melting process of thin films

View Online   Export Citation   CrossMark

Chenyu Jin (金晨羽)[1,2,a]   and Hans Riegler[1,b]

AFFILIATIONS

[1] Max Planck Institute of Colloids and Interfaces, Science Park Golm, 14476 Potsdam, Germany
[2] Physics of Living Matter, Department of Physics and Materials Science, University of Luxembourg, L-1511 Luxembourg City, Grand Duchy of Luxembourg

[a] Author to whom correspondence should be addressed: chenyu.jin@uni.lu
[b] Electronic mail: hans.riegler@mpikg.mpg.de

ABSTRACT

We perform numerical and experimental studies on the melting process of thin films initiated by a small hole in the continuum regime. The presence of a nontrivial capillary surface, namely the liquid/air interface, leads to a few counterintuitive results: (1) The melting point is elevated if the film surface is partially wettable, even with a small contact angle. (2) For a film that is finite in size, melting may prefer to start from the outer boundary rather than a hole inside. (3) More complex melting scenarios may arise, including morphology transitions and the "*de facto*" melting point being a range instead of a single value. These are verified by experiments on melting alkane films between silica and air. This work continues a series of investigations on the capillary aspects of melting. Both our model and analysis approach can be easily generalized to other systems.

I. INTRODUCTION

Thermostability of thin films is of great interest in theory and in practice.[1] For example, it is very important to know when and how an anticorrosion coating, a filter membrane, or a semiconductor layer would collapse under high temperature. Here, the thermostability is characterized by the "*de facto*" melting point of the thin film, which, due to the ineligible interfacial free energies, is different from the melting point of the bulk material.

The most used equation for calculating the "*de facto*" melting point of a confined system is the Gibbs–Thomson equation.[2–5] It predicts that the melting point of a confined system is lower than the bulk melting temperature, with a shift that is inversely proportional to the characteristic length of the confinement. This theory is deduced from a classical two-phase model: a small solid particle covered by its melt, with one solid–liquid interface. The area of this interface varies during melting, hence the interfacial energy varies and contributes to the total free energy change. For thin films, a variation of this model is used, but still only the solid–liquid interface is considered.

However, in most real-life cases, there will be at least one capillary surface, i.e., the liquid–air interface. The prerequisite for the Gibbs–Thomson equation is that the liquid melt covers uniformly

a solid particle floating in the air, so that the capillary surface is a spherical shell that does not change in shape or area. In practice, this means all the facets of the floating particle must be "premelting,"[6,7] i.e., a thin layer of liquid melt covers the solid facets *before* the temperature reaches the bulk melting point.

A bad news is that "premelting" is only confirmed on certain facets of ice and lead (Pb). Experimental study with lead particles shows that the Gibbs–Thomson equation breaks down once a non-premelting facet is involved: The liquid melt wets the facet with a nonzero contact angle.[8] This will also happen when the particle is not floating but in contact with a substrate. Liquid could be pinned at the grain boundaries or wet the substrate with a nonzero contact angle. The shape of the capillary surface will become nontrivial, so does the interfacial energy. For long, it has been known that the effects of capillary surface on melting is complex.[9–13] However, this problem is rarely systematically analyzed.

Previously, we have observed an unexpected melting scenario of molecularly thin terrace of long-chain alkanes: Liquid drops appear at the edge and "eat" into the terrace.[14] We have revealed that the emergence of these drops is due to (1) the coexistence of liquid and solid under equilibrium and (2) the Plateau–Rayleigh instability of the capillary surface.[15] Later, we analyzed the melting behavior of cylindrical aggregates[16] in gaseous environment based

on the same experimental system and showed elevated melting point due to non-premelting facets.

In this work, we study the melting behavior of a thin, planar solid film from a defect in the shape of a cylindrical hole. During melting, the capillary surface may appear in different shapes. We show that (1) the hole inside the film may not be the preferred starting point of melting and (2) if melting starts from the hole, morphology transitions at different instants during the melting will lead to different melting scenarios as well as different "*de facto*" melting points. Although the simulation is based on our experimental system, the long-chain alkane film between air and silica substrate, the model can be easily generalized to other systems.

II. THEORY AND METHODS

A. Quasi-static melting process

We analyze the melting process within a continuum framework. Although the film thickness can be close to the molecular scale, the work of Henrich *et al.* showed that continuum models are adequate for ≥ 2 adjacent liquid monolayers[17] Contributions from the line tension,[18,19] the disjoining pressure,[20] and gravity are neglected. When alkane solid melts, the volume increases typically by $\approx 10\%$.[21] This change in volume can be neglected without affecting our conclusion. We, hence, use the volume of the liquid melt V_l to represent the amount of melted material. Melting is treated as a slow, quasi-static process: Only an infinitesimal change of parameter is applied for the status change. Therefore, the capillary surface is always fully relaxed to the minimum of the interfacial energy (area).

Note that the quasi-static approach is possible in our system because we have observed the coexistence of liquid and solid under (meta-)stable equilibrium.[15,16] This is caused by the existence of non-premelting facets and the nontrivial capillary surface, which is not the case for a bulk system or a Gibbs–Thomson system. In the following, we analyze the melting process in detail.

The system status is determined by the total free energy G_{total}, which is the sum of the bulk energy G_B and the interfacial energies G_I. Figure 1(a) illustrates the total free energy as a function of V_l in an example system. Three different temperatures are chosen: the bulk melting temperature T_0, the "*de facto*" melting temperature T_m, and a temperature in between. Note that at T_0, $G_B = 0$; hence, $G_{\text{total}} = G_I$ (black curves). Each (local) minimum on the energy curve indicates a (meta-)stable equilibrium state, as marked with black crosses. Red crosses mark the unstable equilibrium states, above which the melt will complete without any energy barrier. The gray line connecting the (meta-)stable equilibrium states indicates the quasi-static melting process. It ends when the system reaches the temperature at which only unstable equilibrium is possible. We call this temperature the "*de facto*" melting temperature T_m of the system. In literature, it is sometimes called the "true" or the "critical" melting temperature.

In order to decide the scenario of melting as a quasi-static process, we need to find out the equilibrium curve that plots how the
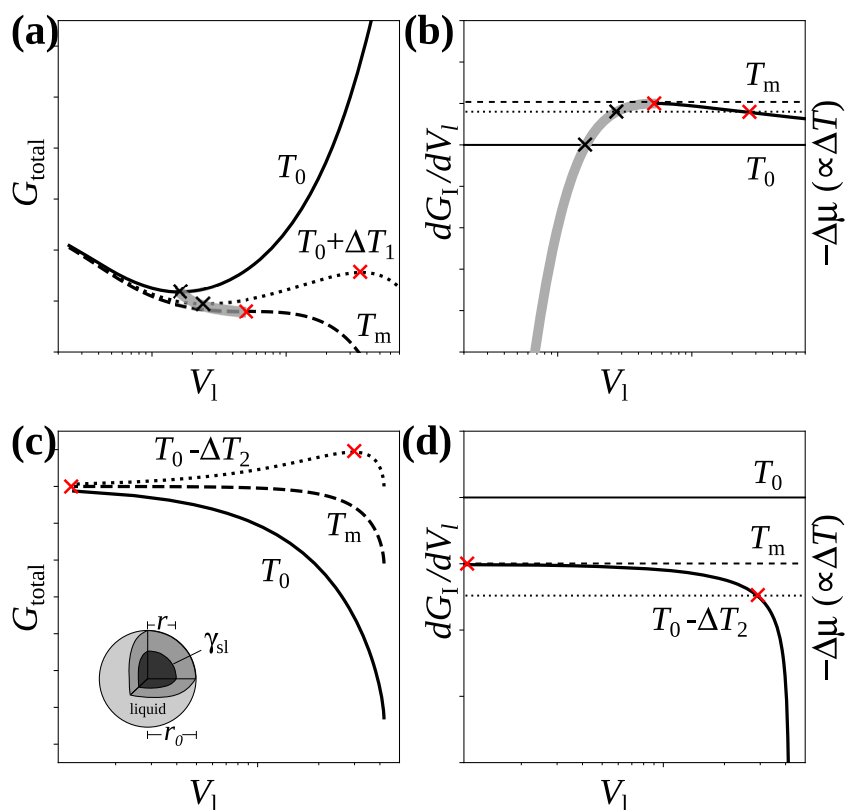
FIG. 1. Free energy change during melting of two typical systems. (a) and (b) correspond to an example system: a film melting from a hole of $r_0/h = 20$. (c) and (d) correspond to the typical Gibbs–Thomson system: a premelting spherical particle with initial radius r_0.

system parameters change from the initial (all solid) to the final state (all liquid). At equilibrium, we have $\partial G_{total}/\partial V_l = 0$, or

$$\Delta\mu + \frac{dG_I}{dV_l} = 0, \qquad (1)$$

where $\Delta\mu$ is the bulk chemical potential difference per volume between liquid and solid under a constant pressure (in this case, 1 bar).

On the one hand, $\Delta\mu$ only depends on the temperature T. More specifically, when the relevant temperature range is small so that a constant melting entropy ΔS_{fus} can be assumed, $\Delta\mu$ at an arbitrary temperature T is calculated as[22,23]

$$\Delta\mu \simeq -\Delta S_{fus} \cdot (T - T_0), \qquad (2)$$

where T_0 is the bulk melting point. That is, $\Delta\mu$ decreases linearly with temperature T.

On the other hand, dG_I/dV_l does not change with T. Rather, it is a function of V_l. The equilibrium curve should hence be plotted with T and V_l as the parameters. From Eqs. (1) and (2), we have the relation

$$\Delta T = T - T_0 = \frac{1}{\Delta S_{fus}} \frac{dG_I}{dV_l}. \qquad (3)$$

In Fig. 1(b), dG_I/dV_l is plotted as a function of V_l. Moreover, for the three typical temperatures in Fig. 1(a), we plot the corresponding $-\Delta\mu$, which is proportional to ΔT. They appear as horizontal lines as $\Delta\mu$ does not depend on V_l. Their intersections with the dG_I/dV_l curve indicate the equilibrium states, as marked by crosses. In particular, the rising part of the dG_I/dV_l curve [gray in Fig. 1(b)] corresponds to the local minima of G_{total} at different temperatures. These are (meta-)stable equilibrium states, hence trace the equilibrium curve that describes the quasi-static process. The maximum of dG_I/dV_l corresponds to the upper temperature limit of the quasi-static melting, namely, the "*de facto*" melting temperature T_m of the system.

In contrast, a typical Gibbs–Thomson system does not have quasi-static melting. Figure 1(c) shows the total free energy as a function of V_l for a small spherical solid particle (radius r_0) covered with liquid melt. Again, three different temperatures are chosen: the bulk melting temperature T_0, the "*de facto*" melting temperature T_m, and a temperature lower than T_m. It could be calculated that $dG_I/dV_l = -2\gamma_{sl}/(r_0^3 - 3V_l/(4\pi))^{-1/3}$, and has the maximum at $V_l = 0$. Hence, there is no (meta-)stable equilibrium. The "*de facto*" melting temperature T_m is characterized by an unstable equilibrium at $V_l = 0$.

B. Simulation details

We focus on the melting of a film between two different media: a substrate and air. Melting of a film between identical media or substrates is either straightforward or closely related. Melting starts at a cylindrical hole (radius r_0) in the film that exposes the substrate. For the simulation, we make the following assumptions:

- The hole in the solid maintains a vertical cylinder geometry. The substrate is planar and the film is of uniform thickness,

hence the cylindrical hole also maintains a constant height h during melting.
- The total volume of solid and liquid together remains constant as the density difference between solid and liquid is neglected.
- The liquid wets completely the lateral surface of the hole, but only partially the film surface and the substrate, with a nonzero contact angle.
- The liquid is pinned at the solid/air/liquid contact line of the hole edge; in other words, there is no fixed contact angle at this line.
- Young's equation holds for contact angles at the liquid/substrate/air contact lines.

Long-chain alkane molecules in solid layers align vertically. Therefore, such a model represents the real case of melting of long-chain alkane film at silica–air interface evolving from holes in the film.

The nontrivial shape of the capillary surface during the melting is solved by relaxing the surface in Surface Evolver[24] with a given V_l and corresponding boundary conditions. For the simulations, we use real data of long-chain alkane systems:[25–27] liquid/air interfacial tension $\gamma_{lv} = 25 \times 10^{-3}$ N/m, γ_{lw}(hole side wall) $= 10 \times 10^{-3}$ N/m, γ_{ls}(film surface and substrate) $= 4 \times 10^{-3}$ N/m, and $\Delta S_{fus} = 5 \times 10^5$ J/Km^{-3}. The contact angle is $\theta_{ls} = 15°$ on both the film surface and the substrate. The model can be easily tuned to simulate different systems. For example, if $\theta_{ls} = 90°$, the model represents not only a film coated on a substrate but also a self-supporting film in the air (after a reflection in the substrate plane).

Figure 2 illustrates different liquid shapes that may emerge during melting. The hole, from where the melting starts, has an initial radius r_0 and a depth h (the film thickness), $r_0 > h$. During melting, when the radius of the hole becomes r, the liquid volume $V_l = \pi h(r^2 - r_0^2)$. Liquid melt will first appear as a symmetric rim at the edge of the hole. More precisely, the capillary surface will be a constant-mean-curvature surface of revolution (Delaunay surface, or rouloid).[28,29] As the liquid volume increases, two different situations are possible: Either there remains an opening exposing part of the substrate ["open" shape, (I)] or the liquid covers the entire substrate ["closed" shape (II)].

The "closed" shape has a geometric limit: The top surface of the liquid is a concave spherical cap whose boundary is pinned at the upper edge, hence the "closed" shape will only appear when sufficient amount of the solid has melted. This limit can be calculated analytically. The radius of the hole has to be larger than a minimum radius r_{min}, which is

$$\frac{r_{min}}{h} = \sqrt{2\left(\frac{r_0}{h}\right)^2 - \frac{1}{3}}. \qquad (4)$$

The "open" shape can be symmetric (rouloid) or nonsymmetric (bulged); see Fig. 3. However, in this system, the bulged shape is only possible with sufficiently large V_l that the system is already unstable; hence, it is not the focus of this work.

In the following plots, we use normalized, dimension-free variables: $\overline{G} = G/(\gamma_{lv} r_0 h)$, $\overline{V} = V/(\pi r_0^2 h)$, $\overline{r} = r/h$, $\overline{dG_I/dV_l} = dG_I/dV_l \cdot h/\gamma_{lv}$, and the in-plane curvature $\overline{\kappa} = \kappa \cdot h$.
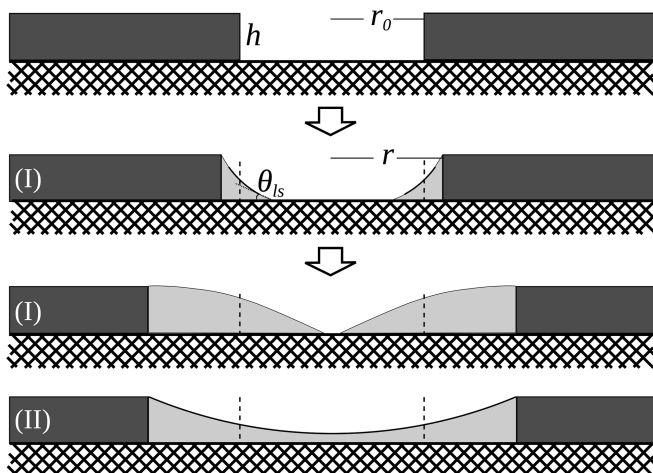
FIG. 2. Melting process from a hole of finite size (r_0) in an infinite film of uniform thickness h. Drawings illustrate the cross section. The liquid wets the lateral surface completely and the substrate partially with contact angle θ_{ls}. Liquid melt first accumulates at the edge as "open" rim (I), then the liquid front coalesces and forms a "closed" concave spherical cap (II).

C. Experimental methods

We use silicon wafer covered with a 300 nm thick oxide layer as substrate. The oxide layer has a refractive index close to the long-chain alkane. Such a thickness is chosen because it provides interference enhancement of contrast from thin alkane layers on the substrate.[30] We coat the piranha-cleaned wafer with long-chain alkane (triacontane $C_{30}H_{62}$ or hexatriacontane $C_{36}H_{74}$) solution in toluene. After a heat–cool cycle, a "surface frozen" alkane monolayer[31] will be formed on the wafer. The sample is then annealed at a temperature slightly below T_0 for a few minutes. Films and islands of various size and height will appear. The suitable ones are chosen for the melting experiments. The height of the alkane films is measured with atomic force microscope (AFM).

The substrate in such a system is actually the surface frozen alkane monolayer, covering the silica surface. This layer, same with the top of alkane film, can only be partially wetted by liquid alkane melt with a contact angle around 15°. This contact angle is directly calculated from microscope observation or alkane droplets: The light (peak wavelength 550 nm) reflected from liquid–air interface and that from the silica–silicon interface in the wafer interfere and form Newton's rings. From this pattern, we get the droplet surface profile and the contact angle.

III. DISCUSSIONS

A. Transitions between different morphologies during melting

Figure 4 plots the normalized interfacial free energy $\overline{G_I}$ and $\overline{dG_I/dV_l}$ against the normalized liquid volume $\overline{V_l}$. The plot represents the melting process of a film from a hole of given size $\overline{r_0} = 5$ on a substrate with $\theta_{ls} = 15°$. This corresponds to the actual case of a hole about 500 nm in radius in an alkane film with $h = 100$ nm.

Note that at the bulk melting temperature T_0, the G_I plot also represents G_{total}. The eventual increase of G_{total} indicates incomplete melting. The minimum at a nonzero V_l indicates a coexistence of liquid melt and the solid under equilibrium. The same can be read from Fig. 4(b): As $\Delta\mu = 0$ at T_0, the intersection of the rising part of the dG_I/dV_l with the x-axis indicates a stable equilibrium.

By Eq. (4), the minimal volume for the "closed" shape $\overline{V_{min}} \approx 1$ (marked by **A**). **B** and **E** mark the two points where the "open" and the "closed" shapes have the same energy. Above **B**, the "closed" shape becomes more favorable; above **E**, the "open" shape becomes more favorable. **C** and **D** mark the two points between which the "open" shape is forbidden.

The melting scenario consists of three stages: (1) melting starts from a symmetric rim; (2) the liquid closes into a concave somewhere between **A** and **C**; (3) the "closed" liquid concave raptures into "open" rim somewhere after **D**. We will ignore the closed-to-open transition in step (3) as it only happens beyond the critical point of melting. Because of an energy barrier between the two shapes, the open-to-closed transition can take place anywhere between **A** and **C**.

In Fig. 4(b), both the "open" and "closed" curves have maxima, corresponding to the upper limit of the quasi-static melting. The respective "*de facto*" melting points and the corresponding "critical" liquid volumes are denoted by (T_m^{open}, V_m^{open}) and $(T_m^{closed}, V_m^{closed})$.

The melting process of films from holes of different sizes is summarized in the phase diagram in Fig. 5, parameterized by $\overline{V_l}$ and $\overline{r_0}$. The phase diagram is divided into three regions where (i) only "open" shape is possible (dark gray), (ii) only "closed" shape is possible (white), and (iii) both shapes are possible (light gray). The boundary between region (i) and region (iii) is derived analytically from Eq. (4). The dashed-dotted curve is the iso-energy curve where "open" and "closed" shapes have the same interfacial energy ($G_I^{closed} = G_I^{open}$).

The melting scenario presented in Fig. 4, with $\overline{r_0} = 5$, corresponds to the vertical straight line, with the marks **A** to **E** bearing the same meanings. We also plot the "critical" volumes V_m^{open} (solid curve) and V_m^{closed} (dotted curve), as indicated in Fig. 4(b).
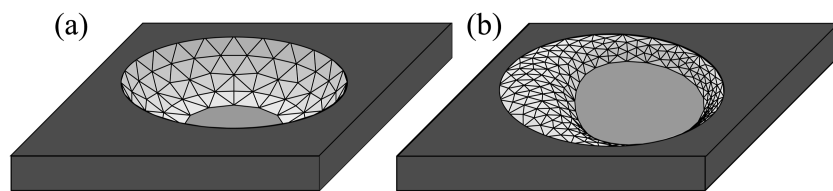
FIG. 3. Two types of "open" morphologies: (a) rouloid, or rotational-symmetric constant-mean-curvature rim, and (b) bulged rim.
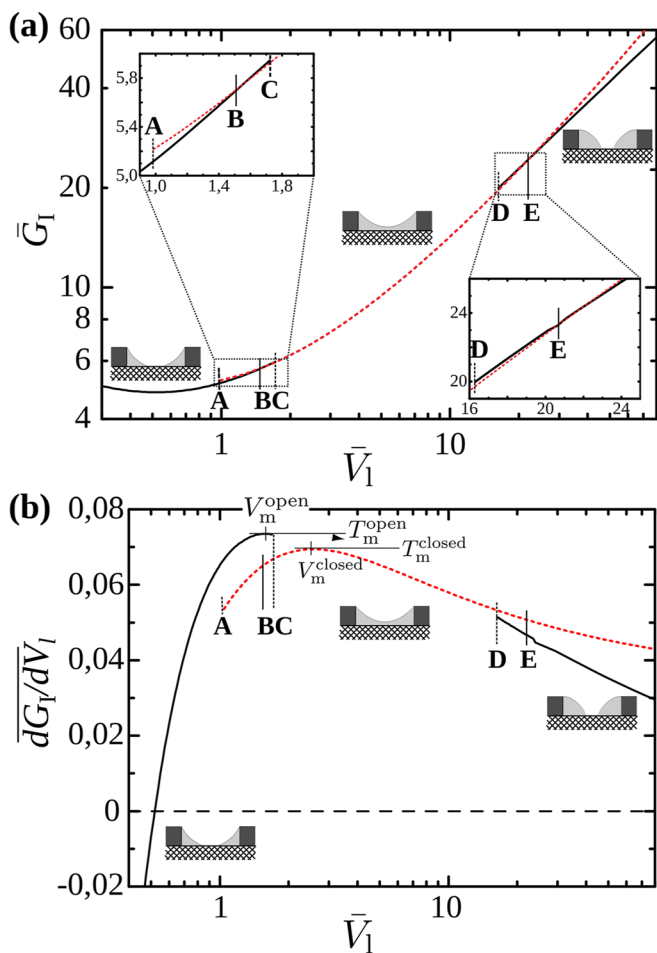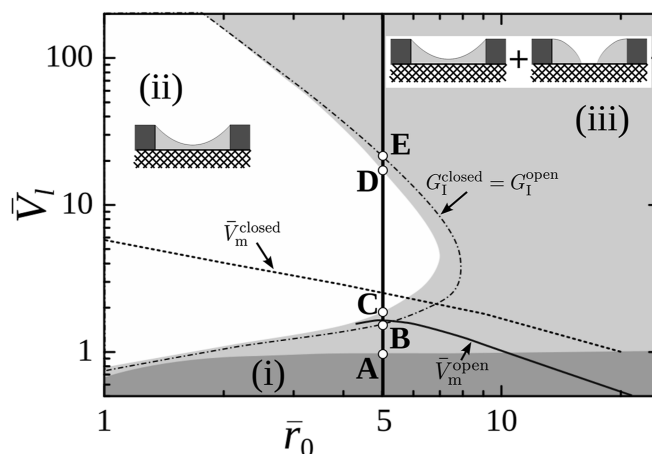
FIG. 4. Melting process of a film from a hole of $\overline{r}_0 = 5$. (a) Normalized interfacial energy $\overline{G}_l$ as a function of normalized liquid volume $\overline{V}_l$. The solid black lines and the dashed red line indicate respectively the "open" and the "closed" shapes. For small volume (left of **A**), only an "open" shape is possible. Between **C** and **D**, only a "closed" shape is possible. Between **A** and **C**, also above **D**, both shapes are possible but with a difference in energy, except when at **B** and **E**, the two iso-energy points. (b) The corresponding $\overline{dG_l/dV_l}$ as a function of $\overline{V}_l$.

FIG. 5. Phase diagram for the two different shapes ("open" and "closed") parameterized by $\overline{V}_l$ and $\overline{r}_0$. The three regions colored differently show where (i) only "open" shape, (ii) only "closed" shape, and (iii) both shapes can exist due to the geometrical boundary conditions. The dashed-dotted curve indicates where the "open" and "closed" shapes have the same interfacial energy. The solid and the dashed curves shows, respectively, the critical volumes of "open" and "closed" shape, i.e., the absolute volume limits of thermal stability. A volume-increasing path is indicated, with the points **A** to **E** same as in Fig. 4.

B. Melting scenarios and blurred melting points

In the following, we look into the melting scenarios for different $\overline{r}_0$, i.e., the film melt from a hole of different given sizes. Figure 6 shows the $\overline{dG_l/dV_l}$ as a function of $\overline{V}_l$ with the same markings as in Fig. 4. Note that for $\overline{r}_0 = 4, 5, 6$, both the "open" and the "closed" curves have rising parts. Therefore, there are two equilibrium curves, each describes a quasi-static melting process. At the overlapping part (**A**–**C**), the system can jump from one equilibrium curve to the other by overcoming an energy barrier.

For $\overline{r}_0 = 4$, melting starts from liquid forming a symmetric rim at the hole edge. Let us assume the morphology transition happens at **B**. From **b1** to **b2**, it will first be an isochoric transition. However, at this temperature, the corresponding liquid volume V_l on the

"closed" curve is much larger, hence V_l will rapidly increase from **b2** to **b3**. The system is still metastable because **b3** is not yet the maximum. Same analysis applies to any point between **A** and **C**; the system is always stable after transition. Hence, the maximum on the "closed" curve, T_m^{closed}, is the only "*de facto*" melting point in this system.

In practice, this melting scenario allows us to seal small holes in the solid film: First, raise the temperature slowly until there is enough liquid inside the hole to form a closed concave while carefully keeping the temperature below T_m^{closed}. Then, quickly freeze the system and solidify the closed concave of liquid melt into a glass state. The hole is sealed.

For $\overline{r}_0 = 5$, the scenario becomes different around the open-to-close transition: If the transition occurs at **A**, it goes from **a1** via **a2** to **a3**, after which the system is still metastable. However, if the transition occurs at **B**, it will lead to complete melting as the temperature at **b1** is already higher than T_m^{closed}. It is also possible that the transition does not occur before the temperature reaches T_m^{open}, the maximum on the "open" curve. In summary, the "*de facto*" melting point T_m of this system is a temperature range rather than a single temperature. It can be any value between T_m^{closed} and T_m^{open}, depending on when the morphology transition takes place.

For $\overline{r}_0 = 6$, even if the transition occurs at the minimum volume (**A**), the temperature is already higher than T_m^{closed}, and the system melts immediately. The "*de facto*" melting point T_m of this system is also a temperature range, but between T_{a1} and T_m^{open}.

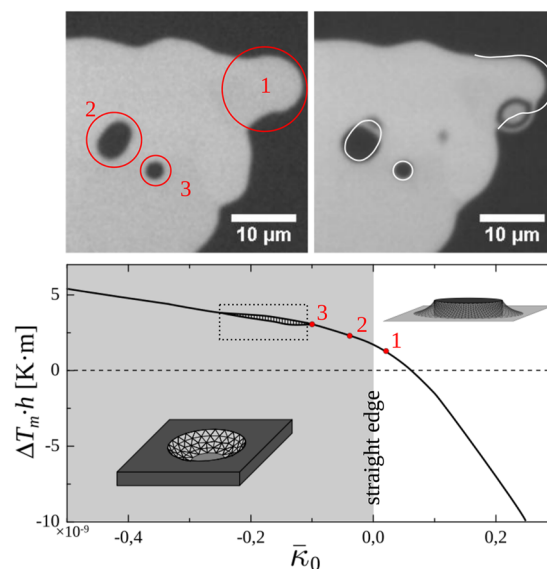In the case of $\overline{r}_0 = 20$, the liquid in the system remains a symmetric rim up to T_m^{open}. "Closed" shape is only possible when V_l exceeds the corresponding liquid volume at T_m^{open}; hence, it is absolutely unstable in the sense of melting.
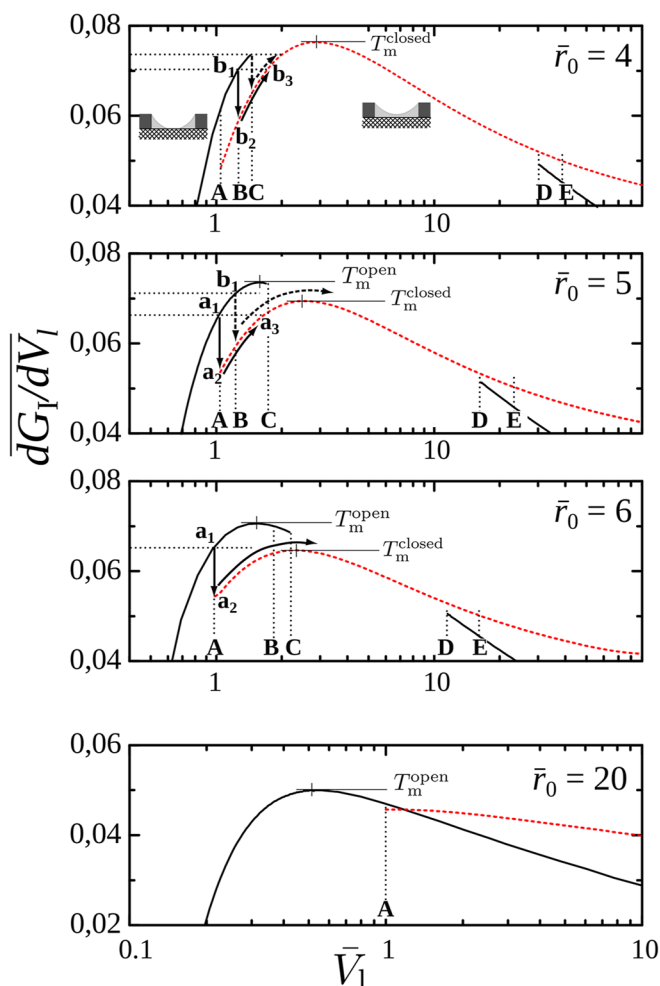
FIG. 6. Melting scenarios of film from holes of different sizes. $\overline{dG_l/dV_l}$ is plotted as a function of $\overline{V_l}$. As discussed in the text, the rising parts are the equilibrium curves that describe the quasi-static melting processes. Same as in Fig. 4, the solid black lines and the dashed red lines indicate correspondingly the "open" rim and the "closed" concave. Point **A** to **E** have also the same meaning. T_m^{open} and T_m^{closed} indicate the "*de facto*" melting points of the corresponding morphology.

FIG. 7. Top: Melting behavior of solid alkane film ($h \approx 100$ nm) with three different local structures: (1) a protruding "peninsula" ($\overline{r_0} \approx 40$, $\overline{\kappa_0} \approx 0.025$); (2) a hole with $\overline{r_0} \approx 30$, $\overline{\kappa_0} \approx -0.033$; (3) a hole with $\overline{r_0} \approx 10$, $\overline{\kappa_0} \approx -0.1$. In the same experiment, they melt sequentially. Bottom: Simulated melting point shift (scaled to the height) of different geometries as a function of initial in-plane curvature (normalized). The model is based on the experimental system of alkane film/island melting. The gray region shows film melting from hole, and the white region shows melting of island. The boundary between the two region indicates melting of a straight terrace edge. The melting point shifts for the three local structures shown in top frame are marked. The dotted rectangle highlights the geometries with "*de facto*" melting points being a range. Bulging, which happens during melting a less-curved structure and lowers T_m, is not shown on this plot.

C. Experimental results of different hole melting scenarios

Combined with our previous calculation on melting of cylindrical island[16] and straight-edge terrace,[15] we have now the full picture of the melting process of different geometries. In Fig. 7 (bottom), we plot the scaled melting point shifts $\Delta T \cdot h$ in our model system as the function of the normalized in-plane curvature of the initial solid edge. We assign a positive in-plane curvature to the island, $\overline{\kappa_0} = h/r_0$, and negative to the holes, $\overline{\kappa_0} = -h/r_0$. One sees the ΔT_m decreases monotonically with the curvature. As a consequence, if a film with irregular edge and holes melts, the melting will start first from the island (peninsula), then the straight edge, and finally the tiny defects

(holes) inside. This counterintuitive sequence of melting is verified by the following experiment.

Figure 7 (top) shows the melting process of an alkane film ($C_{36}H_{74}$) of ~100 nm thickness. The curved edges behave locally like islands, and inside the film, there are two holes of different sizes. The top right panel shows how much solid is melted at different positions under the same temperature. At the "peninsula" (1), compared to the solid boundary before melting (white line), a large amount of solid disappears. The liquid accumulates as a big bulge. Around the big hole (2), some solid melts as well, while around the small hole (3) barely any change can be observed. Such a melting sequence is consistent with the estimated "*de facto*" melting points at these three geometries: The "peninsula" (1) with the lowest "*de facto*" melting point melts the first and the small hole (3) with the highest "*de facto*" melting point melts the last.

Note that this sequence of melting makes it very hard to experimentally measure the melting point shift at a hole. Before the melting starts around the hole, it would have already started from the outer boundary. Then, according to our previous study, the liquid melt would appear as drops that run and "eat" into the film at high speed.[14,15] Hence, the geometry would have been destroyed before any meaningful measurement.

IV. CONCLUSIONS

When the contribution of the capillary surface (liquid/air interface) is taken into consideration, the melting process becomes nontrivial. We present a general approach for analyzing this system. More specifically, we first compute the energy of all the possible configurations with relaxed capillary surfaces, then deduce quasi-static process from the plot of energy derivative.

We apply this approach to thin films with holes of different sizes. We come to interesting conclusions, including an elevated "*de facto*" melting point that in some cases becomes a range and a counterintuitive sequence of melting that starts from outer boundary instead of defects inside. These are verified by experiments on thin films of long-chain alkanes between silica and air.

ACKNOWLEDGMENTS

AUTHOR DECLARATIONS

Conflict of Interest

The authors have no conflicts to disclose.

Author Contributions

Chenyu Jin: Conceptualization (equal); Data curation (lead); Investigation (lead); Methodology (lead); Project administration (lead); Software (lead); Validation (lead); Visualization (lead); Writing – original draft (lead); Writing – review & editing (equal). **Hans Riegler**: Conceptualization (equal); Project administration (supporting); Resources (lead); Supervision (lead); Writing – review & editing (equal).

DATA AVAILABILITY

The data that support the findings of this study are available within the article as plots. Data for generating plots in this study are available from the corresponding author upon reasonable request.

REFERENCES

[1] P. Huber, J. Phys.: Condens. Matter **27**, 103102 (2015).
[2] P. Pawlow, Z. Phys. Chem. **65U**, 1 (1909).
[3] G. Tammann, Z. Anorg. Allg. Chem. **110**, 166 (1920).
[4] F. Meissner, Z. Anorg. Allg. Chem. **110**, 169 (1920).
[5] E. Rie, Z. Phys. Chem. **104U**, 354 (1923).
[6] J. W. M. Frenken and J. F. van der Veen, Phys. Rev. Lett. **54**, 134 (1985).
[7] J. G. Dash, Contemp. Phys. **30**, 89 (1989).
[8] J. J. Métois and J. C. Heyraud, J. Phys. France **50**, 3175 (1989).
[9] N. Maeda and H. K. Christenson, Colloids Surf., A **159**, 135 (1999).
[10] H. K. Christenson, Phys. Rev. Lett. **74**, 4675 (1995).
[11] H. M. Fretwell, J. A. Duffy, M. A. Alam, and R. Evans, J. Radioanal. Nucl. Chem. **210**, 575 (1996).
[12] M. E. Glicksman, A. Lupulescu, and M. B. Koss, "Capillary mediated melting of elliipsoidal needle crystals," in *Free Boundary Problems* (Springer, 2006), pp. 219–230.
[13] S. T. Moerz, K. Knorr, and P. Huber, Phys. Rev. B **85**, 075403 (2012).
[14] P. Lazar and H. Riegler, Phys. Rev. Lett. **95**, 136103 (2005).
[15] H. Kusumaatmaja, R. Lipowsky, C. Jin, R.-C. Mutihac, and H. Riegler, Phys. Rev. Lett. **108**, 126102 (2012).
[16] C. Jin and H. Riegler, J. Phys. Chem. **120**, 16815 (2016).
[17] B. Henrich, C. Cupelli, M. Santer, and M. Moseler, New J. Phys. **10**, 113022 (2008).
[18] R. C. Tolman, J. Chem. Phys. **17**, 333 (1949).
[19] J. K. Berg, C. M. Weber, and H. Riegler, Phys. Rev. Lett. **105**, 076103 (2010).
[20] B. V. Derjaguin and N. V. Churaev, J. Colloid Interface Sci. **66**, 389 (1978).
[21] W. F. Seyer, R. F. Patterson, and J. L. Keays, J. Am. Chem. Soc. **66**, 179 (1944).
[22] C. J. Adkins, *Equilibrium Thermodynamics* (Cambridge University Press, 1983).
[23] J. G. Dash, A. W. Rempel, and J. S. Wettlaufer, Rev. Mod. Phys. **78**, 695 (2006).
[24] K. A. Brakke, Exp. Math. **1**, 141 (1992).
[25] M. Dirand, M. Bouroukba, A.-J. Briard, V. Chevallier, D. Petitjean, and J.-P. Corriou, J. Chem. Thermodyn. **34**, 1255 (2002).
[26] P. Yi and G. C. Rutledge, J. Chem. Phys. **135**, 024903 (2011).
[27] H. Riegler and R. Köhler, Nat. Phys. **3**, 890 (2007).
[28] C. Delaunay, J. Math. Pures Appl. **6**, 309–314 (1841).
[29] J. Eells, Math. Intell. **9**, 53 (1987).
[30] R. Köhler, P. Lazar, and H. Riegler, Appl. Phys. Lett. **89**, 241906 (2006).
[31] C. Merkl, T. Pfohl, and H. Riegler, Phys. Rev. Lett. **79**, 4625 (1997).